**Supporting Information For**

# Embodied carbon in the carbon nitride hollow sphere for enhanced charge separation and photocatalytic water splitting

Lei Luo[a], Jiani Ma[a]*, Haixing Zhu[a], Junwang Tang[b]*

[a] Key Lab of Synthetic and Natural Functional Molecule Chemistry of Ministry of Education, the Energy and Catalysis Hub, College of Chemistry and Materials Science, Northwest University, Xi'an 710127, P. R. China.

[b] Department of Chemical Engineering, University College London, Torrington Place, London WC1E 7JE, UK.

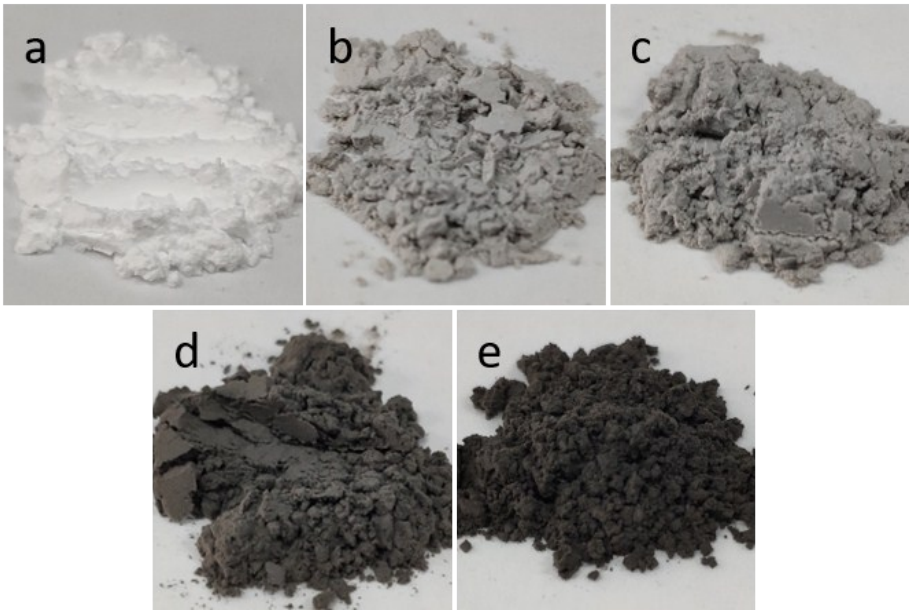


**Figure S1**. Optical images of (a) pristine MCM-41, (b) MCM-41(N600), (c) MCM-41(N700), (d) MCM-41(N800), (e) MCM-41(N900).

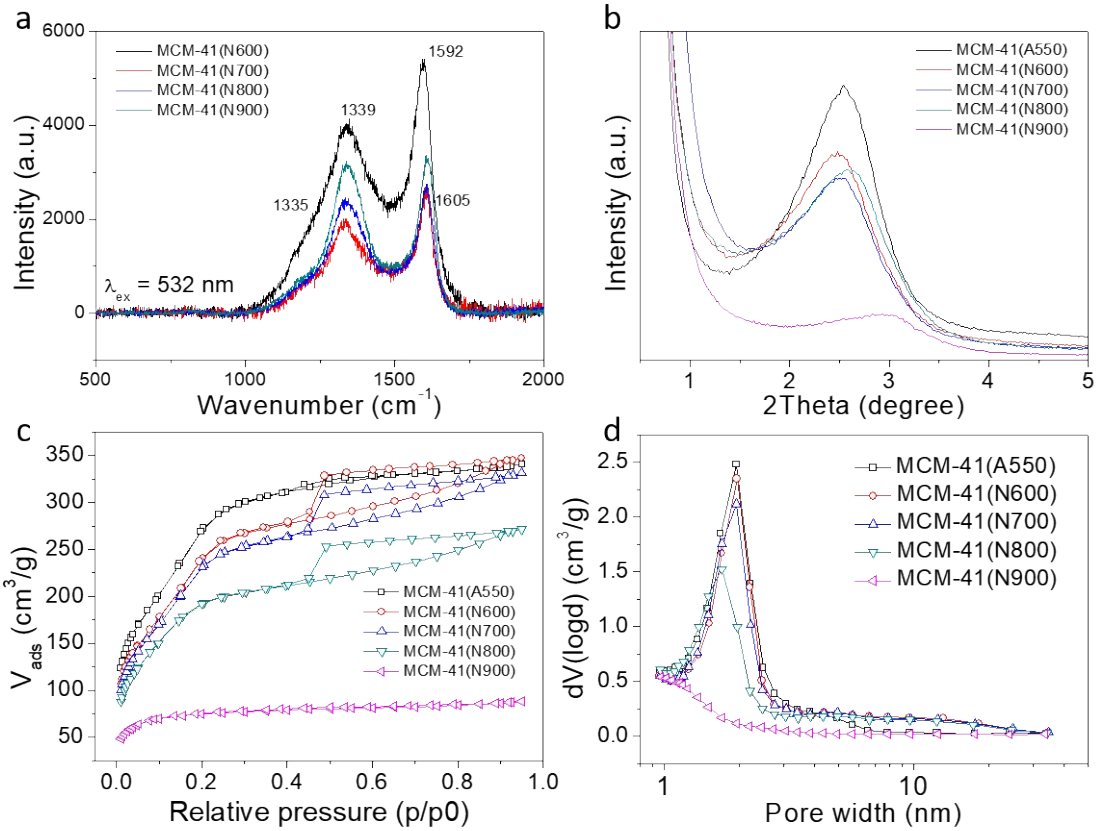


**Figure S2**. (a) Raman spectra, (b) small-angel XRD spectra, (c) $N_2$ physical adsorption-desorption isotherms at 77 K and (d) the pore size distribution of MCM-41 and MCM-41(Nx).

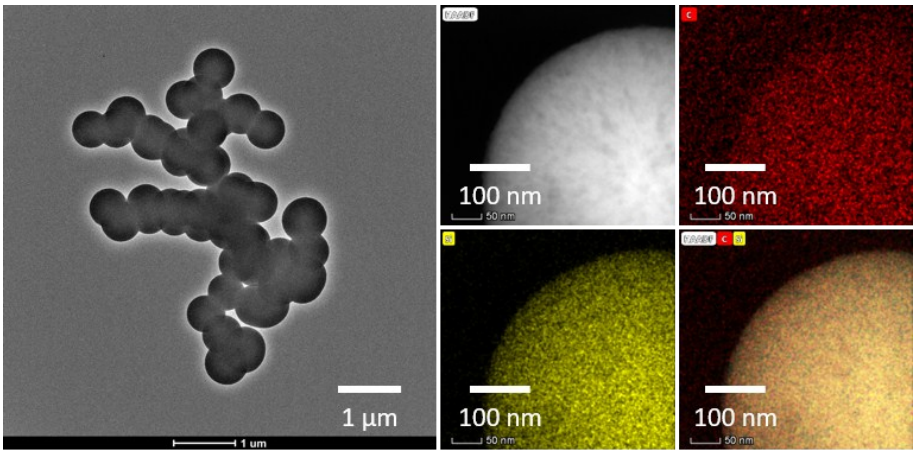


**Figure S3**. TEM and TEM-mapping images of MCM-41(N700).

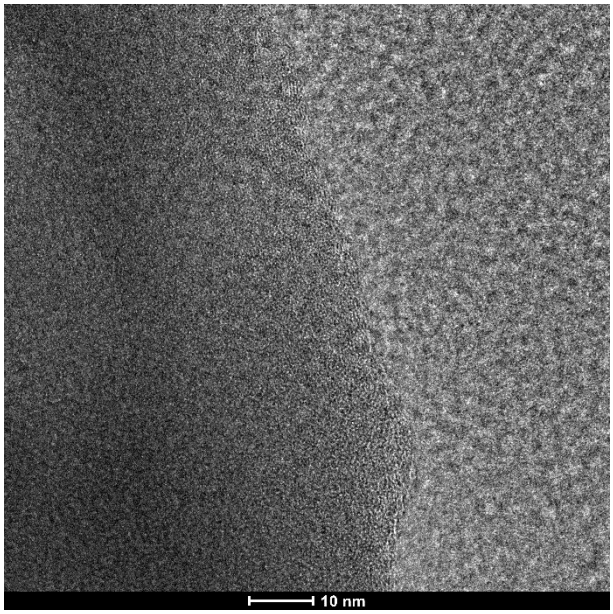


**Figure S4**. HRTEM images of C-GCN700. Due to the low content of graphitic carbon and relatively low crystalline degree of g-$C_3N_4$, no obvious lattice fringes corresponding with the graphitic carbon or g-$C_3N_4$ were observed.

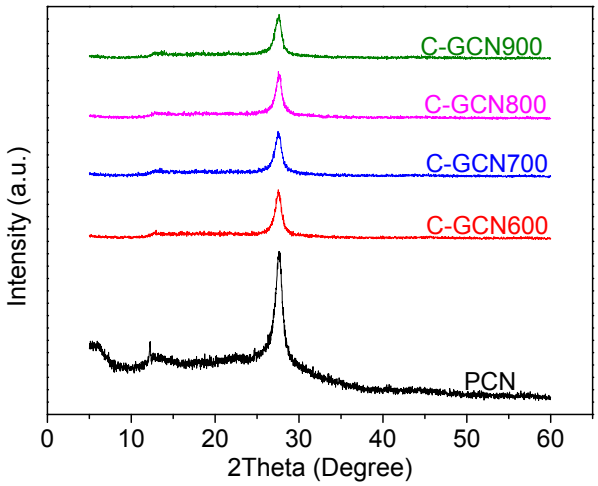


**Figure S5**. XRD patterns of PCN and C-GCNx.

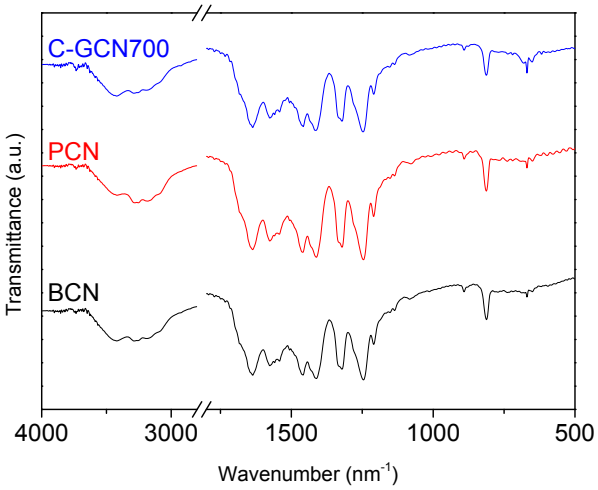


**Figure S6**. FT-IR spectra of BCN, PCN and C-GCN700.

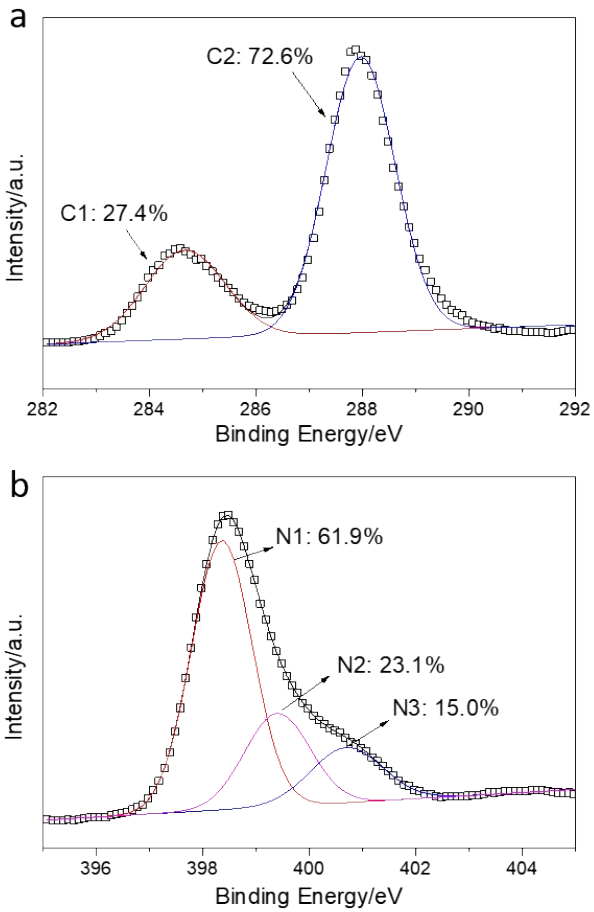


**Figure S7**. (a) C1s and (b) N1s XPS spectra of PCN.

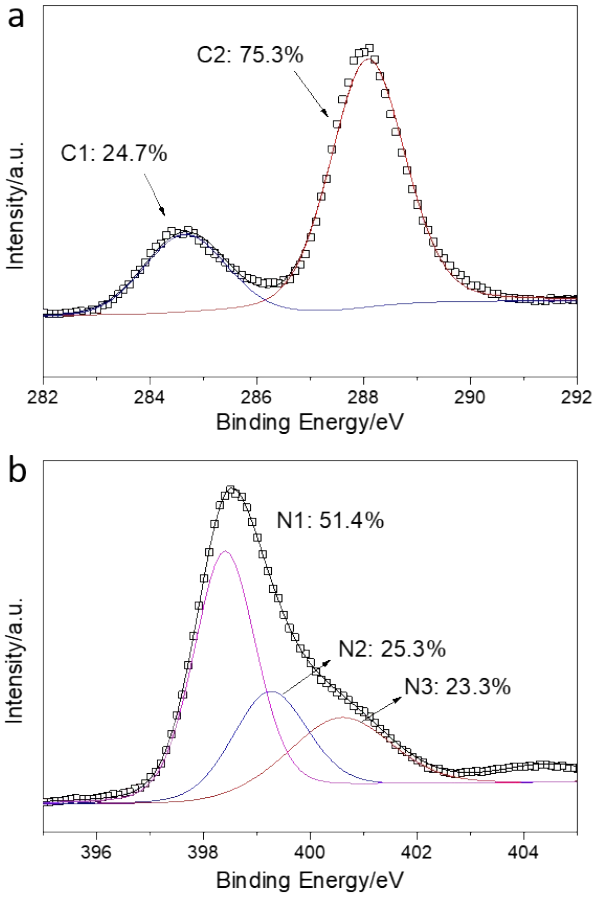


**Figure S8**. (a) C1s and (b) N1s XPS spectra of BCN.

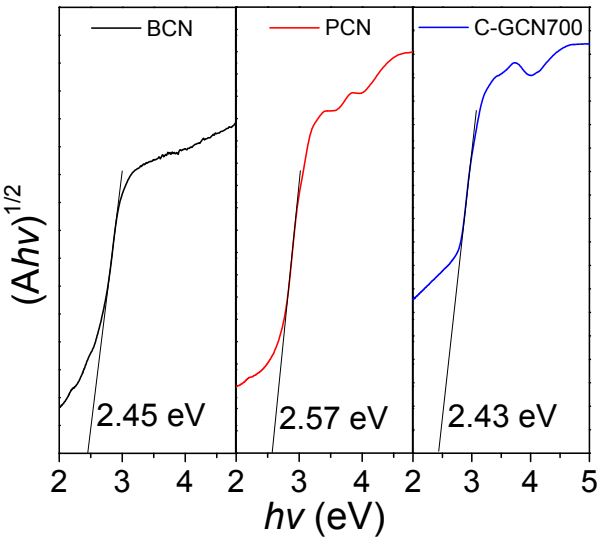


**Figure S9**. Tauc plots of BCN, PCN and C-GCN700.

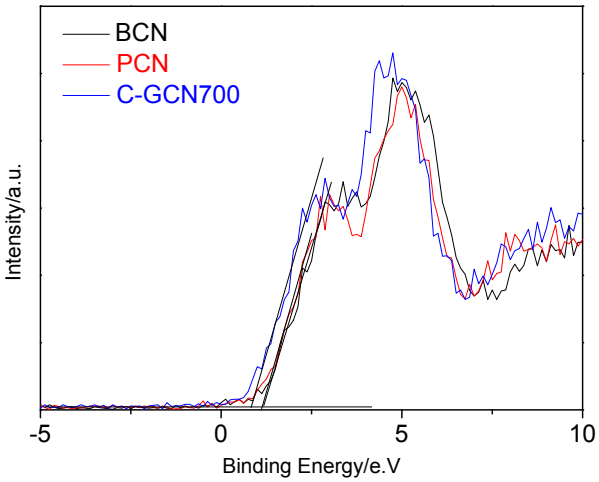


**Figure S10**. XPS-VB spectra of BCN, PCN and C-GCN700.

**Table S1**. Textural properties of the templates: MCM-41 and MCM-41(Nx).

| Sample | $S_{BET}$ | $V_{pore}$[a] | Average pore | $I_D$ | $I_G$ | $I_D/I_G$ | Carbon |
|---|---|---|---|---|---|---|---|

| | ($m^2$/g) | ($cm^3$/g) | width (nm) | | | | content[b] (%) |
|---|---|---|---|---|---|---|---|
| MCM-41 | 1018.4 | 0.53 | 1.94 | / | / | / | 0 |
| MCM-41(N600) | 912.5 | 0.54 | 1.95 | 4132 | 5426 | 0.76 | 1.23 |
| MCM-41(N700) | 867.5 | 0.51 | 1.94 | 2002 | 2743 | 0.73 | 1.37 |
| MCM-41(N800) | 723.0 | 0.42 | 1.69 | 2442 | 2743 | 0.89 | 2.20 |
| MCM-41(N900) | 286.6 | 0.14 | <1 | 3184 | 3349 | 0.95 | 3.05 |

[a] $p/p_0 = 0.95$. [b] Elemental analysis.

**Table S2**. Textural properties of g-$C_3N_4$ vesicles.

| Sample | $S_{BET}$[a] ($m^2 \cdot g^{-1}$) | $V_{pore}$[b] ($cm^3 \cdot g^{-1}$) | C/N molar ratio[c] | Theoretical extra carbon (wt.%) |
|---|---|---|---|---|
| BCN | 12.8 | 0.03 | 0.674 | / |
| PCN | 48.0 | 0.12 | 0.678 | 0.00 |
| C-GCN600 | 78.0 | 0.22 | 0.697 | 1.03 |
| C-GCN700 | 51.8 | 0.12 | 0.704 | 1.37 |
| C-GCN800 | 47.3 | 0.12 | 0.712 | 1.80 |
| C-GCN900 | 30.2 | 0.09 | 0.742 | 3.33 |

[a] BET method. [b] $p/p_0 = 0.95$. [c] Elemental analysis.

**Table S3**. The lifetime of charge carrier obtained from time-resolved PL spectra.

| Sample | $A_1$ (%) | $\tau_1$ (ns) | $A_2$ (%) | $\tau_2$ (ns) | $\tau$ (ns) |
|---|---|---|---|---|---|

| | | | | | |
|---|---|---|---|---|---|
| BCN | 82 | 1.51 | 18 | 7.48 | 2.58 |
| PCN | 79 | 2.01 | 21 | 9.14 | 3.49 |
| C-GCN700 | 74 | 1.94 | 26 | 9.53 | 3.90 |

**Table S4**. The band gap energy, valence band and conduction band position of BCN, PCN, and C-GCN700.

| Sample | *BE* (eV) | $E_V$ (eV) | $E_C$ (eV) |
|---|---|---|---|
| BCN | 2.45 | 1.14 | -1.31 |
| PCN | 2.57 | 1.14 | -1.43 |
| C-GCN700 | 2.43 | 0.86 | -1.57 |